

REVIEW ARTICLE

Review on the synthesis of doped TiO₂ nanomaterials by Sol-gel method and description of experimental techniques

Sankara Rao Miditana^{1,2*}, Siva Rao Tirukkovalluri², Imandi Manga Raju², A. Bangaru Babu¹, A. Ramesh Babu¹

¹ Department of Chemistry, Government Degree College, Puttur, Chittoor, Andhra Pradesh-517583, India

² Department of Inorganic & Analytical Chemistry, A.U. College of Science & Technology, Andhra University, Visakhapatnam, Andhra Pradesh, India-530003

Received: 2022-02-07

Accepted: 2022-04-07

Published: 2022-05-01

ABSTRACT

TiO₂-based nanomaterials are very effective for water and air purification and act as good antibacterial agents due to their unique physicochemical properties. TiO₂ is a promising nanocatalyst because of its non-toxicity, chemical stability, and low cost. The wide band gap and rapid electron-hole recombination limit its performance which can be overcome by doping with metals and non-metal ions. Metal doping improves the trapping of electrons to inhibit electron-hole recombination and non-metal doping reduces the bandgap of TiO₂. These doped TiO₂ materials can be synthesized by different routes like the Sol-gel method, hydrothermal method, precipitation method, impregnation method, etc. Among these, the Sol-gel method is reported as the best and most accurate for the synthesis of TiO₂ particles in the nano scale range. Because it allows the incorporation of dopant ions at the molecular level with homogeneity and high chemical purity. The structural, morphological, and optical properties of as-synthesized TiO₂ nanocatalysts can be well characterized by XRD, SEM, EDX, FT-IR, UV Vis-DRS, TEM, BET, and PL. In this review article, we would like to discuss the advantage of the Sol-gel method over other preparative methods of TiO₂ nanomaterials and experimental techniques related to their characterization.

Keywords: TiO₂ nanomaterials, Sol-gel method, Photocatalyst, SEM, FT-IR, UV-DRS.

How to cite this article

Rao Miditana S., Rao Tirukkovalluri S., Manga Raju I., Bangaru Babu A., Ramesh Babu A. Review on the synthesis of doped TiO₂ nanomaterials by Sol-gel method and description of experimental techniques. J. Water Environ. Nanotechnol., 2022; 7(2): 218-229.

DOI: 10.22090/jwent.2022.02.008

INTRODUCTION

For the remediation of environmental pollution, photoactivity of many metal oxides was studied with a special focus on heterogeneous photocatalytic activity of titanium dioxide (TiO₂) as it exhibits some eye-catching characteristics, such as non-toxicity, chemical stability, and low cost [1-7]. The photocatalytic properties of TiO₂ have been still a concern of many studies and attracted attention in several applications [8-11]. The vanguard and influencing properties of the photocatalytic activity of TiO₂ particles have included the surface

area [12], crystallinity, crystallite size, and crystal structure [13-15]. The photocatalytic property of TiO₂ is restricted only to UV light irradiation, which limits the use of natural sunlight in electromagnetic radiation. Therefore, to improve the catalytic activity in the UV/visible region the properties of TiO₂ particles have been modified and treated with selective surface treatments such as surface chelation, surface derivatization, platinumization, or doping TiO₂ with selective metal and nonmetal ions [16-19]. In recent years, much attention has been paid to enhancing the performance of TiO₂ by doping with metal ions.

* Corresponding Author Email: sraom90@gmail.com

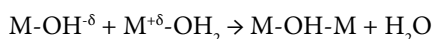


Different methods were designed for fine TiO₂ powder preparation in the literature, some of them are: hydrolysis [20], hydrothermal treatment [21], hydrothermal oxidation [22], impregnation [23], incipient wetness impregnation [24], coprecipitation [25], chemical solution deposition [26], mechanical alloying [27] and sol-gel technique [28-30]. Among these, hydrothermal, coprecipitation, impregnation and sol-gel are widely used methods for TiO₂ photocatalysts preparation. A detailed description of these techniques has been given below.

A. Hydrothermal Synthesis

In the 20th century, hydrothermal synthesis was identified as an important technology for the synthesis of materials, predominantly in the fields of hydrometallurgy and single crystal growth [31].

Hydrothermal synthesis follows the condensation of precursors containing M-OH groups to form polynuclear species which are formed by the elimination of water molecules. The water elimination can be either olation or oxolation.



In olation reaction nucleophilic addition of OH⁻ to hydrated metal cation takes place. Oxolation is a condensation of two OH⁻ groups to form one water molecule which is removed by creating an oxo bridge. Dehydration of olate species leads to oxo-species. Olation is generally faster than oxolation.

In the hydrothermal method, the preparation of nanocrystalline TiO₂ powders use commonly titanium alkoxide and alcohol as precursor solutions and some amount of acid and organic additives are introduced to the solution to bring in crystallization and prevent particle agglomeration [32]. Hence, it is relatively difficult to control the ratio of various compositions to get pure anatase crystallite. Moreover, the TiO₂ powders formed by the hydrothermal method needs repeated washing to remove the organic solvent, additive and they don't usually produce homogeneous and high surface area materials [33, 34].

Hydrothermally synthesized nanosized material results in the well crystalline phase and thermal stable nanosized products. Kominami et al. synthesized nanosized titanium (IV) dioxide in the anatase form by hydrolysis of titanium (IV) alkoxide in toluene and water that was dissolved from the gas phase at high temperatures (150–300

°C) [34, 35]. Chen et al. also have prepared TiO₂ nanocrystalline powders by a similar method [36].

There are difficulties in applying this method during the metal doping process to get the desired pure anatase crystallite, such that controlling the ratio of various components, utilizing expensive autoclaves, and the difficulty observing crystal growth are limitations of this method. Generally, it involves large quantities of solution and longer processing time, even though they are characterized by forming well-controlled morphology [21]. Changing pH can also lead to protonation or deprotonation, hence catalyst formation can occur only in a limited range of pH. It also needs a higher temperature during synthesis (above 150 °C).

B. Precipitation Method

Precipitation is the formation of a solid in a solution or inside another solid during a chemical reaction or by diffusion in a solid. When the reaction occurs in a liquid, solid products are formed as a precipitate, or when compacted by a centrifuge, it is called a pellet.

In solids, precipitation occurs if the concentration of one solid is above the solubility limit in the host solid, due to rapid quenching or ion implantation, and the temperature is high enough that diffusion can lead to segregation into precipitates. Precipitation in solids is routinely used to synthesize nanoclusters [37].

Stages of precipitation are three, namely: supersaturation, nucleation, and growth. Nucleation depends on the ratio of existing concentration to the concentration under equilibrium conditions. At higher concentrations, supersaturation occurs and therefore, nucleation can take place with further growth to produce a gel. The formed gel is aged, filtered, washed, dried, and finally calcined.

The precipitation method was used by different researchers for the synthesis of TiO₂ nanoparticles. These precipitation methods involve the precipitation of hydroxides by the addition of a basic solution (NH₄OH, NaOH, and urea) to raw material, followed by crystallization of the oxide and finally calcination [38]. Weeraman Buraso *et al.* synthesized titanium dioxide nanoparticles by a simple precipitation method using titanium (IV) isopropoxide as a starting material [39]. Zhinuo Wang et al. synthesized TiO₂ nanoparticles by two different precipitation methods using titanium tetrachloride (TiCl₄) and titanium oxalate [Ti(C₂O₄)₂] as raw materials and

tested its photocatalytic activities [40]. Roussin Lontio Fomekong et al. synthesized Co³⁺ doped TiO₂ nanoparticles by a facile co-precipitation method and used it for gas sensing applications [41].

Limitation of the precipitation method includes the failure to manage the ratio of components during metal doping since the limiting step in the process is the diffusion of the species, precipitation of multiple species with different solubility under the same temperature and dilution can pose a problem in the case of co-precipitation during the co-doping process. The different concentration gradients of the species also cause additional problems [25]. Since precipitation requires more solvent and precipitation agents, it also added more costs for catalyst separation and waste disposal.

C. Impregnation method

There are two main impregnation methods are discriminated, namely, wet impregnation, whereby an excess amount of solution is used, and pore volume impregnation, the seal porosity in metal casting, powder metal parts, and electrical components are typically performed by one of the following four different processes: Dry vacuum and pressure, Wet vacuum and pressure, Wet vacuum and internal impregnation or pressure impregnation method. Choosing the best process depends on a variety of factors such as the number and amount of porosity contained in the parts, desired sealing results, and economics.

The dry vacuum and pressure method requires the highest investment in equipment yet provides the best results when sealing porosity that is very small and sealing requirements are more stringent. This method uses a pressure vessel or autoclave and a resin storage vessel. Components are placed into the autoclave and a vacuum is applied. The level of vacuum is generally between 28 to 29.5 inches of Hg. The vacuum is held until the air is removed from the autoclave and from within the porosity. Next, the sealant which is stored in the separate vessel is transferred, usually via a pipe, from the storage vessel to the autoclave. The transfer is facilitated by differential pressure. As the sealant is being transferred, the vacuum is maintained. When the sealant reaches a level approximately 6 inches above the components in the autoclave, the transfer is complete. The residual vacuum is released into the atmosphere and pressure is then applied. The pressure is held for some time long

enough to facilitate penetration into the porosity. After the desired time under pressure, the sealant is transferred back to the storage tank, again through the use of differential pressure. The autoclave is finally vented to the atmosphere and the yields are removed, washed, and cured.

The wet vacuum pressure impregnation method requires a relatively high investment in equipment yet may not produce the highest quality results of a dry vacuum pressure method. The wet vacuum and pressure method uses a single pressure vessel or autoclave but no storage tank. The sealant is stored in the autoclave. Parts are immersed in the sealant within the autoclave and a vacuum is applied. The level of vacuum is generally between 28 to 29 inches of Hg. The rest procedure is similar to that of the dry vacuum and pressure method. The internal impregnation or pressure impregnation method requires the least investment in equipment and provides excellent sealing results in even the finest porosity. The internal impregnation or pressure impregnation method utilizes the part as the vessel. This method, although quite effective, allows only one component to be processed at a time. To internally impregnate apart, the vessel is first filled with sealant while venting any trapped air. The sealant within the vessel is then pressurized up to the test pressure. The pressure is typically held until the sealant is observed weeping. When this is achieved, the pressure is reduced in the atmosphere and the sealant is drained from the vessel.

Many investigators have studied the photocatalytic activities of nanocatalysts doped with metal ions using impregnation methods. The semiconductor photocatalyst (Fe-TiO₂) was prepared by a simple wet impregnation method by Sathishkumar et al. [42]. Wang et al. [43] also prepared the ZnO-anatase-rutile semiconductor by impregnating the ZnO nano-particle on the Degussa P25 surface. Based on the economic consideration, Lin et al. [44] demonstrated that the visible-responsive photocatalyst, Pt/TiO₂, can be easily synthesized by a sol-gel process or by an impregnation method to load PtOx on TiO₂.

The drawback of the above method includes that it is more appropriate for doping on supporting materials and is not suitable for the preparation of catalyst powders in solution. It is also difficult to keep the homogeneous distribution of dopant in the nanocatalyst during its preparation. Also, a large volume of aqueous water is involved in the process and the product obtained requires repeated

washing and heat treatment for a long time, which makes the process tedious. These methods also require a relatively high investment in equipment to produce the highest quality results.

D. Sol-gel Method

The sol-gel technology was in use since about the mid-1800s and was used almost after a century by the Schott Glass Company (Jena, Germany) [45]. Sol-gel technology was used in the synthesis of new materials for catalysis [46, 47], chemical sensors [48], membranes [49, 50], fibers [51], optical gain media [52], photochromic applications [53] and solid-state electrochemical devices [54, 55]. It is also used in scientific and engineering fields, such as the ceramic industry [45], nuclear industry [45], and electronic industry [56].

The advantages derived from preparing TiO₂ by sol-gel method [57-59], include synthesis of nanosized crystallized powder of high purity at relatively low temperature, the possibility of stoichiometry controlling process, preparation of composite materials, and production of homogeneous materials. These benefits attracted many researchers to the use of the method in preparing TiO₂-based photocatalysts. Different kinds of literature also show that the use of the sol-gel method for various purposes like applying the dip coating, spin-coating, or spray pyrolysis techniques to deposit TiO₂ films, moreover, it has several advantages, such as low cost, simple apparatus set up and the possibility to control the properties of the film through the solution composition [60].

The sol-gel method is also used to prepare supported metal catalysts and catalyst supports with higher thermal stability and higher resistance to deactivation while allowing for more flexible control of the catalyst properties, such as particle size, surface area, and pore size distribution. It has an additional inherent advantage of allowing the production of materials directly cast upon substrates [61, 62]. This method involves the formation of TiO₂ sol-gel by hydrolysis and condensation of titanium alkoxides.

Based on these advantages of the method and the prospect of the method for synthesis of different catalysts which would be environmentally and friendly applied to degrade hazardous materials, the author selected the sol-gel technique from the rest of the available methods.

Mechanism of the sol-gel process

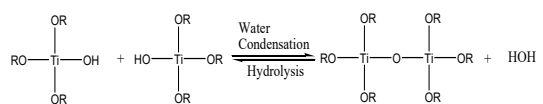
The sol-gel process involves the evolution of inorganic networks through the formation of a colloidal suspension (sol) and gelation of the sol to form a network in a continuous liquid phase (gel) [63]. The precursors for synthesizing these colloids consist of a metal or metalloid element surrounded by various reactive ligands. Metal alkoxides are most popular for this purpose, hence they react readily with water. The most widely used metal alkoxides are the alkoxysilanes and other alkoxides such as aluminates, titanates, and borates are commonly used in the sol-gel process.

At the functional group level, three reactions generally take place to describe the sol-gel process: hydrolysis, alcohol condensation, and water condensation. These general reaction schemes are given in the following equations 1, 2, and 3.

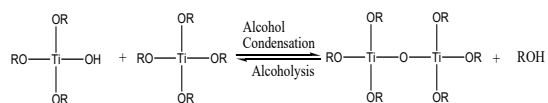
1) Hydrolysis of an alkoxide titanate



2) Water condensation reaction to form a titanate network.



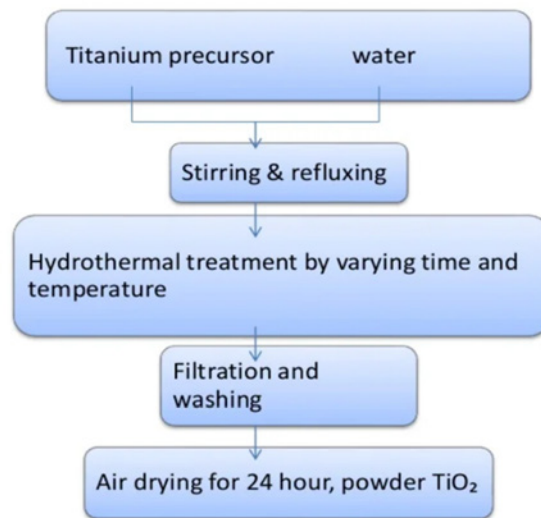
3) Alcohol condensation reaction to form a titanate network.



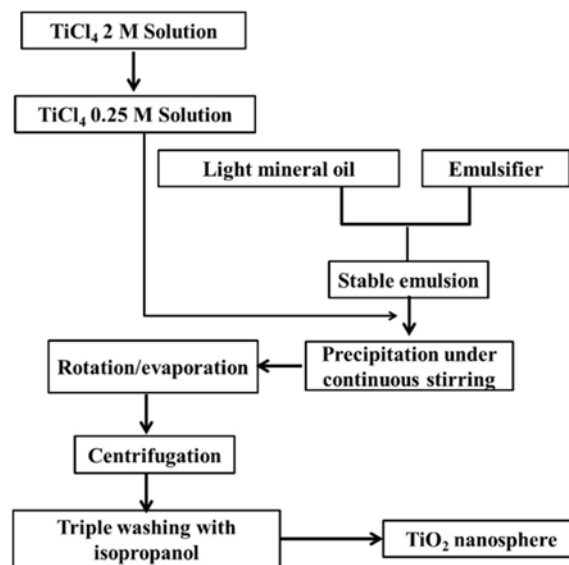
Generally, the hydrolysis reaction (eq.1), through the addition of water, replaces alkoxide groups (OR) with hydroxyl groups (OH). Subsequent condensation reactions (eq.2. and eq.3.) involving the titanol groups (Ti-OH) produce Titoxane bonds (Ti-O-Ti) plus the by-products of water or alcohol.

Description of Experimental Techniques for Characterization of Catalyst

After the synthesis of TiO₂ nanomaterial by the sol-gel method, following different instrumental



Scheme 1. Schematic representation of Hydrothermal synthesis route for the preparation of nanocrystalline TiO₂



Scheme 2. Schematic representation of precipitation synthesis route for the preparation of TiO₂ nanoparticles

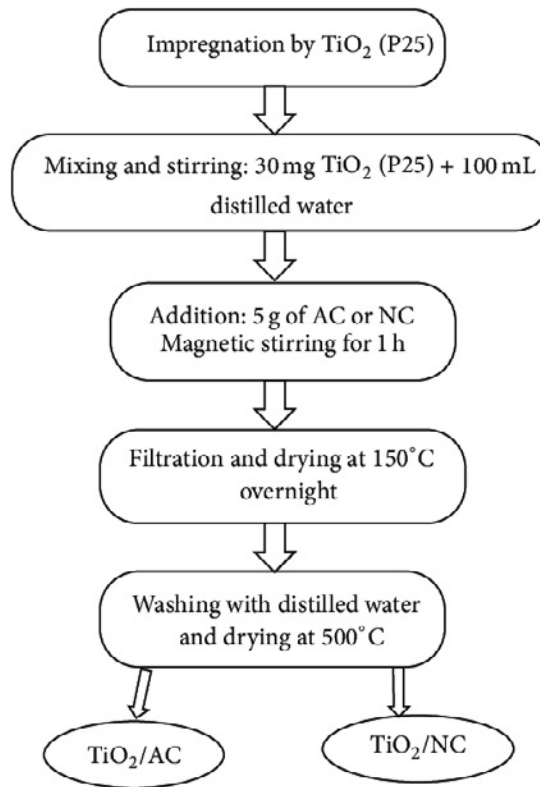
techniques were used for their structural, morphological, and optical characterization.

A. X-ray Diffraction method (XRD)

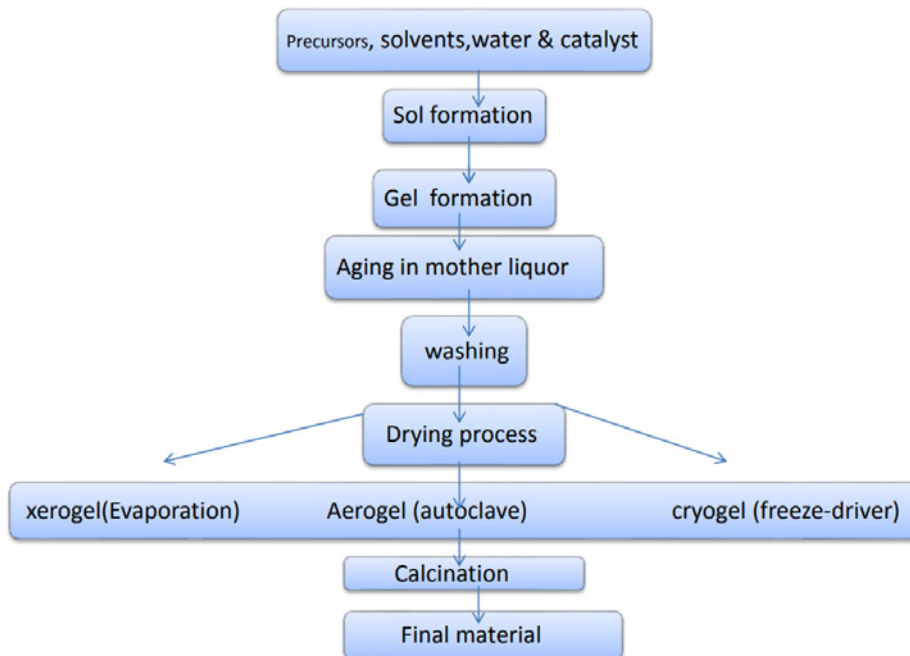
X-ray is a short wavelength part of electromagnetic radiation (10 pm-10 nm) discovered by Wilhelm Roentgen in 1895 [64]. X-ray powder diffractometry involves the characterization of material by understanding

the atomic arrangement in the crystal lattice. The technique uses single or multiple phase specimens comprising a random orientation of small crystallites each with the order of 1-50 μm in diameter. Each crystallite in turn is made up of a regular, orderly arranged array of atoms.

Each signal in the X-ray spectrum corresponds to a Bragg reflection (**Fig.1**), a mathematical representation (Bragg's law) of how X-ray or other



Scheme 3. Schematic representation of impregnation synthesis route for the preparation of TiO₂ nanoparticles



Scheme 4. Schematic representation of sol-gel synthesis route for the preparation of TiO₂ nanoparticles

electromagnetic wave undergoes diffraction in crystal planes.

$$n\lambda = 2d\sin\theta$$

Where d is the distance between crystal planes, θ is the angle of incidence of the X-ray beam with the crystal plane, λ is the wavelength of the X-ray and n is an integer usually assigned a value of 1.

In the present study, X-ray diffraction measurement was carried out with an X-ray diffractometer (Model Ultima IV, RIGAKU) using CuK α ($\lambda = 0.154059$ nm) radiation with a nickel filter. The applied current and voltage were 40 mA and 40 kV, respectively. The 2θ scanning range was 5° to 90° with a scan rate of 2 min^{-1} . The diffraction of X-rays by crystal planes is shown in Fig.1.

B. UV-Visible Diffuse Reflectance Spectroscopy (UV-vis. DRS)

Diffuse Reflectance Spectroscopy (DRS) is a spectroscopic technique based on the reflection of light in the ultraviolet (UV), visible (VIS), and near-infrared (NIR) region by a powdered sample. Kortum [65] has discussed the theoretical and practical principles of diffuse reflectance in great detail in his book.

In a UV-vis.DRS spectrum the ratio of the light scattered from an infinitely thick layer and the scattered light from an ideal non-absorbing reference sample is measured as a function of the wavelength, λ . The illumination of powdered samples by incident radiation leads to diffuse illumination of the samples. The incident light is

partially absorbed, partially scattered. The scattered radiation, emanating from the sample is collected in an integration sphere and detected.

In the present study, the diffuse reflectance spectra (DRS) were recorded with a Shimadzu 3600 UV-Visible NIR spectrophotometer equipped with an integrating sphere diffuse reflectance accessory, using BaSO₄ as reference scatter. Powder samples were loaded into a quartz cell and spectra were collected in the range of 200-900 nm.

C. Scanning Electron Microscopy (SEM)

Scanning with SEM is accomplished by the two pairs of electromagnetic coils located within the objective lens [66]. One deflects the beam in the x-direction across the sample and the other pair deflects it in the y-direction. Scanning is controlled by applying an electrical signal to one pair of scan coils, such that the electron beam strikes the sample to one side of the center axis of the lens system. By varying the electrical signal to this pair of coils (x-coils) as a function of time, the electron beam moved in a straight line across the sample and then returned to its original position.

After the line scan, the other set of coils (y.coils in this case) is used to deflect the beam slightly, and the scanning of the beam using the x coils is repeated. Thus, by rapidly moving the beam, the entire sample surface can be irradiated with the electron beam. The image of the sample is produced by using the output of a detector. Samples that conduct electricity are easier to study, for non-conducting samples, a metallic film produced by sputtering with metals like gold, palladium, or

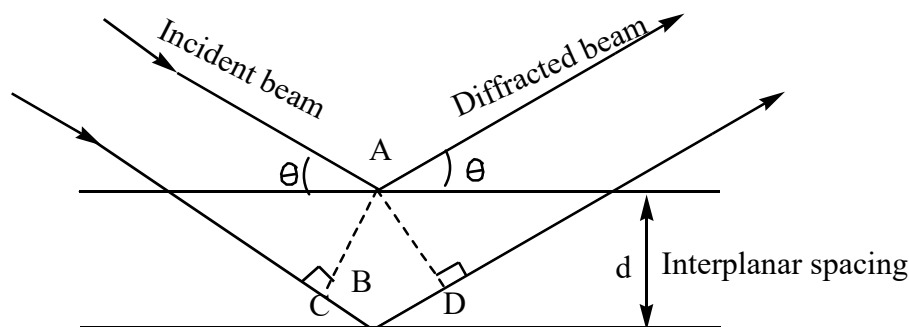


Fig. 1. Diffraction of X-rays by crystal planes.

platinum is employed to make samples conductive for SEM application.

In the present study scanning electron micrographs (SEM) of the prepared catalysts were recorded by the JSM-6610 LV model which is equipped with an energy dispersive X-ray (EDX) spectrophotometer and operated at 20kV.

C. Transmission Electron Microscopy (TEM)

Transmission Electron Microscope utilizes energetic electrons to provide morphology, compositional and crystallographic information on samples at a maximum potential magnification of 1 nanometer. TEM is mainly used for the analysis of particle size along with structure, texture, and shape. Ernest Ruska developed the first electron microscope, a TEM, with the assistance of Max knolls in 1931 [67]. During the same year, Rein holds an electrostatic lens electron microscope [68].

TEM produces a high-resolution, black and white image from the interaction that takes place between prepared samples and energetic electrons in the vacuum chamber. Air is pumped out of the vacuum chamber, creating a space where electrons can move. The electrons then pass through multiple electromagnetic lenses. These solenoids are tubes with a coil wrapped around them. The beam passes through the solenoids, down the column, and makes contact with the screen where the electrons are converted to light and form an image. The image can be manipulated by adjusting the voltage of the gun to accelerate or decrease the speed of electrons as well as changing the electromagnetic wavelength via the solenoids. The coils focus images onto a screen or photographic plates.

TEM images of synthesized nanomaterials were taken using a TECNAI FE12 TEM (Eindhoven, The Netherlands) instrument operating at 120 kV. In each image, more than 100 particles were analyzed with cool ruler software to measure the particle size.

D. N₂ Adsorption-Desorption (BET) Surface Area

BET theory aims to explain the physical adsorption of gas molecules on a solid surface and serves as the basis of an important analysis technique for the measurement of the specific surface area of a material. In 1938, Stephen Brunauer, Paul Hugh Emmett, and Edward Teller published an article about the BET theory [69].

Gas sorption (both adsorption and desorption)

at the clean surface of dry solid powders is the most popular method for determining the surface area of these powders. In a gas sorption experiment, the material is heated and degaussed by vacuum force or inert gas purging to remove adsorbed foreign molecules. Controlled doses of inert gas, such as nitrogen, krypton, or argon, are introduced and the gas is adsorbed or withdrawn and desorbed. The sample material is placed in a vacuum chamber at a constant and very low temperature and subjected to a wide range of pressures, to generate adsorption and desorption isotherms. The amounts of gas molecules adsorbed or desorbed are determined by the pressure variations due to the adsorption or desorption of the gas molecules by the material (the adsorbent). Various amounts of gas molecules will be adsorbed or desorbed at different molecules and using an adsorption model, the total surface area of the material can be determined.

In this study, the Brunauer-Emmett-Teller (BET) surface area was determined from the N₂ adsorption-desorption isotherm at 77.3 K by using a Quantachrome Nova 2200 E system. The sample was outgassed for 3 h at 300 °C before the adsorption.

E. Fourier Transform Infrared Spectroscopic (FT-IR) Studies

The infrared spectrum of a compound is energy absorption in the infrared region of electromagnetic radiation and it is obtained by plotting the percent absorbance or transmittance of IR radiation as a function of wavelength. IR spectroscopy is usually divided into three regions as near IR region (12500 cm⁻¹ - 4000 cm⁻¹), middle IR also known as fundamental vibration region (4000 cm⁻¹ - 667 cm⁻¹) and far IR also known as pure rotational region (667 cm⁻¹ -50 cm⁻¹) [70].

The IR of solid samples would be better handled by the technique popularly known as KBr pelleting [71]. In this technique, a milligram of the finely ground samples is mixed with 100 mg dried KBr powder by using a mortar and pestle. The mixture is then pressed by pelleting machine with about 3 tons to prepare a transparent thin disk. The disk is then held in the instrument beam for spectroscopic examination.

The infrared spectra of prepared samples in this study were recorded with Thermo Nicolet Nexus 670 Spectrometer with a resolution of 4 cm⁻¹ in KBr pellets.

F. Photoluminescence Spectroscopy (PL)

Photoluminescence (PL) is light emission from any form of matter after the absorption of photons (electromagnetic radiation). Photoluminescence spectroscopy is a contactless, nondestructive method of probing the electronic structure of materials. Light is directed onto a sample, where it is absorbed and imparts excess energy into the material in a process called *photo-excitation*. This excess energy is dissipated by the sample through the emission of light or *luminescence*. In the case of photo-excitation, this luminescence is called *photoluminescence*.

Photo-excitation causes electrons within a material to move into permissible excited states. When these electrons return to their equilibrium states, the excess energy is released and may include the emission of light (a radiative process) or may not (a nonradiative process). The energy of the emitted light (photoluminescence) relates to the difference in energy levels between the two-electron states involved in the transition between the excited state and the equilibrium state. The quantity of the emitted light is related to the relative contribution of the radiative process.

Periods between absorption and emission may vary: ranging from short femtosecond-regime for emission involving free-carrier plasma in inorganic semiconductors [72] up to milliseconds for phosphorescent processes in molecular systems, and under the special circumstances delay of emission may even be minutes or hours.

An excitation wavelength is selected by one monochromator, and the luminescence is observed through a second monochromator, usually positioned at 90° to the incident light to minimize the intensity of scattered light reaching the detector. If the excitation wavelength is fixed, the emitted radiation is scanned, and an emission spectrum is produced.

Photocatalytic Reactor

The schematic representation of the photocatalytic reactor used for the degradation of dyes in visible light simulation with synthesized photocatalysts is given in Fig.2. The general photocatalytic degradation procedure was carried out with a required amount of catalyst added to a fresh 100 mL aqueous dye solution of required concentration in a Pyrex glass vessel of 150 ml with continuous stirring.

Cut-off filter 51,472 was placed in the path of light for complete removal of UV radiation and running water was circulated in the sample container to filter IR radiation and to keep the reaction mixture at room temperature. Before irradiation, the solution with catalyst was stirred in the dark for 30 minutes to ensure the establishment of adsorption-desorption equilibrium of dye on the catalyst surface.

The solution was then irradiated with the high-pressure mercury vapor lamp (400W, Osram) with a UV filter which was used as a visible light source (output is 436 - 546 nm) with 35000 lumens and placed 20 cm away from the photoreactor. Approximately (5mL) aliquots of the samples were withdrawn from the solution by using a Millipore syringe (0.45 μm) at certain time intervals and analyzed for the dye concentration. The schematic representation of the photo reactor is shown in Fig. 2.

The percentage degradation of the dye was calculated by using the undermentioned equation.

$$\% \text{ of Degradation} = (1 - A_t/A_0) \times 100$$

Where A_0 is the initial absorbance of dye solution before exposure and A_t is the absorbance of dye solution at time t .

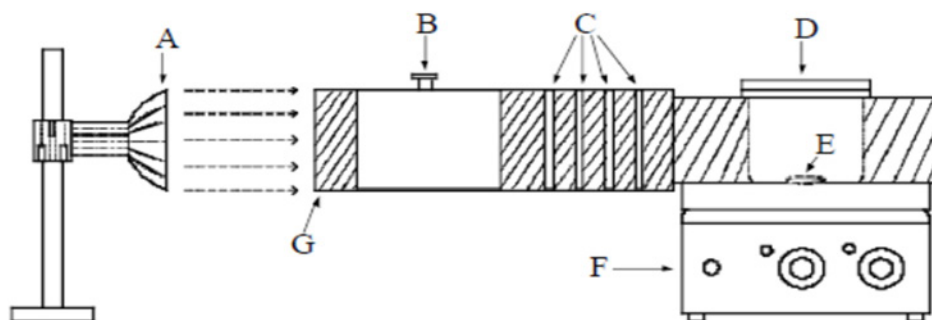


Fig. 2. Schematic representation of photo reactor. (A) light source; (B) UV filters; (C) circulating water (D) beaker with sample solution; (E) magnetic paddle; (F) magnetic stirrer; (G) light channel

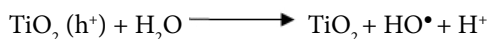
Photocatalytic mechanism for photodegradation of pollutants

The reactive catalyst particles play a key role in the production of hydroxyl radicals (HO•) for the degradation of pollutants [73]. The photocatalytic mechanism by co-doped TiO₂ is briefly represented as follows.

The following steps are the prime steps for the formation of •OH. Its formation is an important step in the photocatalytic degradation of pollutants and the anti-bacterial activity of photocatalyst. When co-doped TiO₂ nanopowder is irradiated with visible light, the electrons get excited to the conduction band leaving behind the holes in the valence band. The recombination of the generated electrons and holes must be prevented for the effective utilization of the catalyst. Thus, generated electrons are captured by the doped dopant ions preventing their recombination.



The holes react with surface-bound hydroxyl groups or with water adsorbed on the surface of TiO₂ to produce hydroxyl radicals and hydrogen ions.



The electrons are transferred to adsorbed oxygen-producing superoxide anion.



These superoxide anions further react with adsorbed water molecules producing peroxide radicals and hydroxyl ions.



The peroxide radicals combine with H⁺ resulting in the formation of hydroxyl radicals and hydroxyl ions. Hydrogen peroxide is formed as an intermediate product.



Holes oxidize these hydroxyl ions to hydroxyl

radicals. Thus, all the species facilitate the formation of HO•. The strong oxidants HO• reacts with pollutant and degrade them.



Thus, the formation of hydroxyl radicals and their role in photocatalytic activity plays an essential role in the degradation mechanism.

CONCLUSIONS

In this review, we discussed various routes of preparation of TiO₂ materials like the sol-gel method, hydrothermal method, precipitation method, and impregnation method. Among these, we highlighted the Sol-gel method as it reported remarkable results due to its advantages i.e synthesis of nanosized crystallized powder of high purity at relatively low temperature, the possibility of stoichiometry controlling process, preparation of composite materials, and production of homogeneous materials with controlled particle size and shape. Various characterization techniques used for structural, morphological, and optical properties of TiO₂ nanomaterials and their photocatalytic activity mechanism for the degradation of pollutants are discussed.

CONFLICT OF INTEREST

The authors declare no conflict of interest.

REFERENCES

- Ikram M, Hassan J, Raza A, Haider A, Naz S, Ul-Hamid A, Haider J, Shahzadi I, Qamar U and Ali S. Photocatalytic and bactericidal properties and molecular docking analysis of TiO₂ nanoparticles conjugated with Zr for environmental remediation. RSC Adv. 2020; 10: 30007. <https://doi.org/10.1039/D0RA05862A>
- Hoffmann M.R, Martin S.T, Choi W and Bahnemann D.W. Environmental applications of semiconductor photocatalysis. Chem. Rev. 1995; 95 (1): 69-96. <https://doi.org/10.1021/cr00033a004>
- Peral J and Ollis D. F. Heterogeneous photocatalytic oxidation of gas-phase organics for air purification: acetone, 1-butanol, butyraldehyde, formaldehyde and m-xylene oxidation, J.Catal, 1992 ;136(2): 554-565. [https://doi.org/10.1016/0021-9517\(92\)90085-V](https://doi.org/10.1016/0021-9517(92)90085-V)
- Zorn M.E, Tomp D.T, Zeltner W.A and Anderson M.A. Photocatalytic oxidation of acetone vapor on TiO₂/ZrO₂ thin films. Appl. Catal. B: Env. 1999; 23 :1-8. [https://doi.org/10.1016/S0926-3373\(99\)00067-3](https://doi.org/10.1016/S0926-3373(99)00067-3)
- Brezova and Stasko A. Spin trap study of hydroxyl radicals formed in the photocatalytic system TiO₂-water-p-cresol-oxygen. J. Catal. 1994; 147: 156-162. <https://doi.org/10.1006/jcat.1994.1125>
- Rekoske J.E and Barteau M.A. Kinetics and selectivity of 2-propanol conversion on oxidized anatase TiO₂. J. Catal. 1997; 165:57-72. <https://doi.org/10.1006/jcat.1997.1467>
- Zhang L.C, Cai K.F and Yao X. Preparation, characteriza-

- tion and photocatalytic performance of Co/Ni co-doped TiO₂ nanopowders. *J. Electroceram.* 2008; 21 :512 -518. <https://doi.org/10.1007/s10832-007-9227-y>
8. Ashfaq, A., Ikram, M., Haider, A. et al. Nitrogen and Carbon Nitride-Doped TiO₂ for Multiple Catalysis and Its Antimicrobial Activity. *Nanoscale Res Lett* 16, 119 (2021). <https://doi.org/10.1186/s11671-021-03573-4>
 9. Ollis D.F, Pelizzetti E and Serpone N. *Photocatalysis Fundamentals and Applications*, John Wiley and Sons, New York, 1989.
 10. Ikram M, Umar E, Raza A, Haider A, Naz S, Ul-Hamid A, Haider J, Shahzadi I, Hassan J, and Ali S. Dye degradation performance, bactericidal behavior and molecular docking analysis of Cu-doped TiO₂ nanoparticles. *RSC Adv.* 2020; 10: 24215-24233 <https://doi.org/10.1039/D0RA04851H>
 11. Khalid N.R., Hussain M.K., Murtaza G, Murtaza G, Ikram M, Ahmad M and Hammad A. A Novel Ag₂O/Fe-TiO₂ Photocatalyst for CO₂ Conversion into Methane Under Visible Light. *J Inorg. Organomet. Polym.* 2019; 29: 1288-1296. <https://doi.org/10.1007/s10904-019-01092-5>
 12. Ohtani B, Zhang S, Handa J, Kajiwara H, Nishimoto S and Kagiya T. Photocatalytic activity of titanium (N) oxide prepared from titanium(N) tetra-2-propoxide: reaction in aqueous silver salt solutions. *J. Photochem. Photobiol. A: Chem.*1992; 64: 223-230. [https://doi.org/10.1016/1010-6030\(92\)85109-8](https://doi.org/10.1016/1010-6030(92)85109-8)
 13. Ohtani B, Ogawa Y and Nishimoto S.I. Photocatalytic Activity of Amorphous-Anatase Mixture of Titanium(IV) Oxide Particles suspended in Aqueous Solutions. *J. Phys. Chem. B.* 1997;101: 3746-3752. <https://doi.org/10.1021/jp962702+>
 14. Tanaka K, Capule M.F.V and Hisanaga T. Effect of crystallinity of TiO₂, on its photocatalytic action. *Chem. Phys. Lett.* 1991; 187 (1, 2): 73-76. [https://doi.org/10.1016/0009-2614\(91\)90486-S](https://doi.org/10.1016/0009-2614(91)90486-S)
 15. Ohtani B, Handa JI, Nishimoto S.I and Kagiya T. Highly Active Semiconductor Photocatalyst: Extra-fine Crystallite of Brookite TiO₂ for Redox Reaction in Aqueous Propan-2-ol and/or Silver Sulfate Solution. *Chem. Phys. Lett.* 1985;120: 292-294. [https://doi.org/10.1016/0009-2614\(85\)87060-3](https://doi.org/10.1016/0009-2614(85)87060-3)
 16. Ikram M, Ali S, Murray R, Hussain A, Islah-u-din, Ismat Shah S. Influence of fullerene derivative replacement with TiO₂ nanoparticles in organic bulk heterojunction solar cells. *Current Applied Physics.* 2015; 15: 48-54. <https://doi.org/10.1016/j.cap.2014.10.026>
 17. Aqeel M, Ikram M, Imran M, Ul-Hamid A, Qumar U, Shahbaz A, Ikram M and Saeed A. TiO₂ Co-doped with Zr and Ag shows highly efficient visible light photocatalytic behavior suitable for treatment of polluted water. *RSC Adv.* 2020; 10: 42235. <https://doi.org/10.1039/D0RA08718A>
 18. Zahid R, Manzoor M, Rafiq A. et al. Influence of Iron Doping on Structural, Optical and Magnetic Properties of TiO₂ Nanoparticles. *Electron. Mater. Lett.* 2018; 14: 587-593. <https://doi.org/10.1007/s13391-018-0060-z>
 19. Saleem A, Imran M, Shahzadi A, Junaid M, Majeed H, Rafiq A. Drastic improvement in catalytic, optical and visible-Light photocatalytic behavior of cobalt and nickel doped TiO₂ nanopowder. *Mater. Res. Express* 2019; 6: 015003. <https://doi.org/10.1088/2053-1591/aae28e>
 20. Duncan J.F and Richards R.G. Hydrolysis of titanium (IV) sulphate solutions, 2 Solution equilibria, kinetics and mechanism, *New Zeal, J. Sci.* 1976; 19: 179-184.
 21. Furlong D.N and Parfitt G.D. Electrokinetics of Titanium Dioxide. *J. Colloid Interface Sci.* 1978;65 (3) : 548-554. [https://doi.org/10.1016/0021-9797\(78\)90107-8](https://doi.org/10.1016/0021-9797(78)90107-8)
 22. Qian Y, Chen Q, Chen Z, Fan C and Zhou G. Preparation of Ultrafine Powders of TiO₂ by Hydrothermal H₂O₂ Oxidation Starting from Metallic Ti. *J. Mater. Chem.* 1993; 3: 203-205. <https://doi.org/10.1039/jm9930300203>
 23. Sakthivel S, Shankar M.V, Palanichamy M, Arabindoo B, Bahnemann D and Murugesan V. Enhancement of photocatalytic activity by metal deposition: characterization and photonic efficiency of Pt, Au and Pd deposited on TiO₂ catalyst. *Water Research.* 2004;38: 3001-3008. <https://doi.org/10.1016/j.watres.2004.04.046>
 24. Mohammad M.M and Al-Esaimi M.M J. Molec. Characterization, adsorption and photocatalytic activity of V doped TiO₂ and sulphated TiO₂ (rutile) catalysts: Degradation of Methylene blue dye. *Cata. Chem.* 2006; 255: 53-58. <https://doi.org/10.1016/j.molcata.2006.03.071>
 25. Ranjit K.T and Viswanathan B. Synthesis, Characterization and Photocatalytic Properties of Iron-doped TiO₂ Catalysts. *J. Photochem. Photobiol. A Chem.*1997; 108: 79-84. [https://doi.org/10.1016/S1010-6030\(97\)00005-1](https://doi.org/10.1016/S1010-6030(97)00005-1)
 26. Yao W.F, Wang H, Xu X.H, Zhou J.T, Yang X.N, Zhang Y and Shang S.X. Photocatalytic property of bismuth titanate Bi₂Ti₂O₇. *Appl. Catal. A. Gen.* 2004; 259(1): 29-34. <https://doi.org/10.1016/j.apcata.2003.09.004>
 27. Kim D.H, Hong H.S, Kim S.J, Song J.S and Lee K.S. Photocatalytic behaviors and structural characterization of nanocrystalline Fe-doped TiO₂ synthesized by mechanical alloying. *J. Alloy. Comp.* 2004; 375: 259-265. <https://doi.org/10.1016/j.jallcom.2003.11.044>
 28. Ying J.Y and Sun T. Research Needs Assessment on Nanostructured Catalysts. *J. Electroceram.*1997; 1 (3) 219-238. <https://doi.org/10.1023/A:1009931726749>
 29. Castillo S, Moran-Pineda M, Molina V, Gomez R and Lopez T. Catalytic reduction of Nitric Oxide on Pt and Rh Catalysts Supported on Alumina and Titania Synthesis by Sol-Gel Method. *Appl. Catal. B: Environ.*1998; 15: 203-209. [https://doi.org/10.1016/S0926-3373\(97\)00047-7](https://doi.org/10.1016/S0926-3373(97)00047-7)
 30. Sullivan W.F and Coles S.S. Thermal Chemistry of Colloidal Titanium Dioxide. *J. Am. Ceram. Soc.*1995; 42 (3) :127. <https://doi.org/10.1111/j.1151-2916.1959.tb14079.x>
 31. Byrappa K and Yoshimura M. *Handbook of Hydrothermal Technology*, Noyes Publications/William Andrew Publishing LLC, U.S.A. 2001. <https://doi.org/10.1016/B978-081551445-9.50003-9>
 32. Basca R.B and Gratzel M. Rutile formation in hydrothermally crystallized nanosized titania. *J. Am. Ceram. Soc.* 1996; 79 (8): 2185-2188. <https://doi.org/10.1111/j.1151-2916.1996.tb08956.x>
 33. Wang C and Ying J.Y. Sol-Gel Synthesis and Hydrothermal Processing of Anatase and Rutile Titania Nanocrystals. *Chem. Mater.* 1999;11: 3113-3120. <https://doi.org/10.1021/cm990180f>
 34. Kominami H, Kato J.I, Takada Y, Doushi Y, Ohtani B, Nishimoto S.I, Inoue M, Inui T and Kera Y. Novel Synthesis of Microcrystalline Titanium (IV) Oxide Having High Thermal Stability and Ultra-High Photocatalytic Activity: Thermal Decomposition of Titanium (IV) Alkoxide in Organic Solvents. *Catal. Lett.* 1997; 46: 235-240. <https://doi.org/10.1023/A:1019022719479>
 35. Kominami H, Murakami S, Kera Y and Ohtani B. Titanium (IV) Oxide Photocatalyst of Ultra-high Activity: a New Preparation Process Allowing Compatibility of High Adsorptivity and Low Electron-Hole Recombination Probability. *Catal. Lett.* 1998;56 :125-129.
 36. Chen Q.W, Qian Y.T, Chen Z.Y, Zhou G.E and Zhang Y.H. Preparation of TiO₂ powders with different morphologies by an oxidation hydrothermal combination method. *Mater. Letts.* 1995;22:77-79. [https://doi.org/10.1016/0167-577X\(94\)00227-4](https://doi.org/10.1016/0167-577X(94)00227-4)
 37. Dhara S. Formation, dynamics, and characterization of nanostructures by ion beam irradiation, *Critical reviews in solid state and materials sciences.* 2007; 32(1,2): 1-50. <https://doi.org/10.1080/10408430601187624>
 38. Poznyak S.K, Kokorin A.I and Kulak A.I. Effect of electron and hole acceptors on the photo electrochemical behavior of nanocrystalline microporous TiO₂ electrodes. *J. Electroanal. Chem.* 1998; 442: 99-105. [https://doi.org/10.1016/S0022-0728\(97\)00458-0](https://doi.org/10.1016/S0022-0728(97)00458-0)

39. Weeraman Buraso¹, Vichuda Lachom¹, Porntip Siriyal and Paveena Laokul. Synthesis of TiO₂ nanoparticles via a simple precipitation method and photocatalytic performance. *Mater. Res. Express.* 2018; 5: 115003. <https://doi.org/10.1088/2053-1591/aadbf0>
40. Zhinuo Wang, Shimin Liu, Xin Cao, Sumei Wu, Chaoqian Liu, Gang Li, et al. Preparation and characterization of TiO₂ nanoparticles by two different precipitation methods. *Ceramics International.* 2020; 46:15333-15341. <https://doi.org/10.1016/j.ceramint.2020.03.075>
41. Lontio F.R. and Saruhan B. Synthesis of Co³⁺-Doped TiO₂ by Co-precipitation Route and Its Gas Sensing Properties. *Front. Mater.* 2019; 6: 252. <https://doi.org/10.3389/fmats.2019.00252>
42. Sathishkumar P, Anandan S, Maruthamuthu P, Swaminathan T, Zhou M and Ashokkumar M. Synthesis of Fe³⁺ doped TiO₂ photocatalysts for the visible assisted degradation of an azo dye. *Physicochem. Eng. Aspects.* 2011; 375: 231-236. <https://doi.org/10.1016/j.colsurfa.2010.12.022>
43. Wang H, Wu Z, Liu Y and Sheng Z. The characterization of ZnO-anatase-rutile three-component semiconductor and enhanced photocatalytic activity of nitrogen oxides. *J. Molec. Catal. A: Chem.* 2008; 287: 176-281. <https://doi.org/10.1016/j.molcata.2008.03.010>
44. Lin Y.M, Tseng Y.H, Huang J.H, Chao C.C, Chen C.C and Wang I. Photocatalytic activity for degradation of nitrogen oxides over visible light responsive titania based photocatalysts. *Environ. Sci. Technol.* 2006; 40 :1616-1621. <https://doi.org/10.1021/es051007p>
45. Brinker C.J and Scherer G.W. *Sol-gel Science: The Physics and Chemistry of Sol-gel Processing*, Academic Press, Boston, MA, (1990).
46. Oye G, Glomm W.R, Vralstad T, Volden S, Magnusson H, Stocker M and Sjoblom. Synthesis, functionalization and characterization of mesoporous materials and sol-gel glasses for applications in catalysis, adsorption and photonics. *J Adv. Colloid. Interface Sci.* 2006; 123: 17-23. <https://doi.org/10.1016/j.cis.2006.05.010>
47. Maduraiveeran G and Ramaraj R. A Facile Electrochemical Sensor Designed from Gold Nanoparticles Embedded in Three-Dimensional Sol-Gel Network for Concurrent Detection of Toxic Chemicals. *Electrochem. Commun.* 2007; 9: 2051-2055. <https://doi.org/10.1016/j.elecom.2007.05.021>
48. Carmona N, Herrero E, Llopis J and Villegas M. Chemical sol-gel based sensors for evaluation of environmental humidity. *A Sensors Actuators B.* 2007; 126: 455-460. <https://doi.org/10.1016/j.snb.2007.03.030>
49. Brinker C.J, Raman N.K, Logan M.N, Sehgal R, Assink R.A, Hua D.W and Waed T.L. Permeation properties of microporous carbon and silica membranes. *J. Sol-gel Sci. Tech.* 1995; 4(2):117-133. <https://doi.org/10.1007/BF00491678>
50. Yang Y.N and Wang P. Preparation and characterizations of a new PS/TiO₂ hybrid membranes by sol-gel process. *Polymer.* 2006; 47 :2683-2688. <https://doi.org/10.1016/j.polymer.2006.01.019>
51. Li X, Gong S and Zeng Z. Development of a Sol-Gel procedure for Preparation of a Diglycidyl ether [4] arene Solid-Phase Microextraction Fiber with Enhanced Extraction Efficiency. *Chromatographia.* 2005; 62: 519-525. <https://doi.org/10.1365/s10337-005-0665-x>
52. Jeronimo P.C.A, Araujo A.N, Conceica M and Montenegro B.S.M. Optical sensors and biosensors based on sol-gel films, *Talanta.* 2007; 72: 13-27. <https://doi.org/10.1016/j.talanta.2006.09.029>
53. Volkan M, Stokes D.L and Vo-Dinh T. A sol-gel derived AgCl photochromic coating on glass for SERS chemical sensor application, *Sensors and Actuators. B: Chemical.* 2005; 106 (2): 660. <https://doi.org/10.1016/j.snb.2004.09.019>
54. Dunn B, Farrington G.C and Katz B. Sol-Gel Approaches for Solid Electrolytes and Electrode Materials. *Solid State Ionics.* 1994; 70: 3-10. [https://doi.org/10.1016/0167-2738\(94\)90281-X](https://doi.org/10.1016/0167-2738(94)90281-X)
55. Skaarup S, West K, Zachau B-Christiansen, Popal M, Kappel J, Kron J, Eichinger G and Semrau G. Towards solid state lithium batteries based on ORMOCER electrolytes. *Electrochim. Acta.* 1998; 43 (10) :1589-1593. [https://doi.org/10.1016/S0013-4686\(97\)10058-5](https://doi.org/10.1016/S0013-4686(97)10058-5)
56. Phani A.R, Passacantando M and Santucci S. Synthesis and characterization of hafnium oxide and hafnium aluminate ultra-thin films by a sol-gel spin coating process for microelectronic applications. *J. Non-Crystal. Solids.* 2007; 353-663. <https://doi.org/10.1016/j.jnoncrysol.2006.10.041>
57. Crisan M, Braileanu A, Raileanu M, Zaharescu M, Crisan D, Dragan N, Anastasescu M, Ianculescu A, Nitoi I, Marinescu V.E and Hodoroaga S.M. Sol-gel S-doped TiO₂ materials for environmental protection. *J. Non-Cryst. Solids.* 2008; 354: 705-709. <https://doi.org/10.1016/j.jnoncrysol.2007.07.083>
58. Liao D.L, Badour C.A and Liao B.Q. Preparation of nano-sized TiO₂/ZnO composite catalyst and its photocatalytic activity for degradation of methyl orange. *J. Photochem. Photobiol. A: Chem.* 2008; 194 (1) :11-19. <https://doi.org/10.1016/j.jphotochem.2007.07.008>
59. Zhang X and Liu Q. Preparation and characterization of titania photocatalyst co-doped with boron, nickel, and cerium. *Mater. Lett.* 2008; 62: 2589-2594. <https://doi.org/10.1016/j.matlet.2007.12.061>
60. Sabataityte J, Oja I, Lenzmann F, Volobujeva O and Krunk M C. R. Characterization of nanoporous TiO₂ films prepared by sol-gel method. *Chimie.* 2006; 9 : 708-712. <https://doi.org/10.1016/j.crci.2005.05.019>
61. Lenzi G.G, Lenzi M.K, Baesso M.L, Bento A.C, Jorge L.M.M and Santos O.A. A. Cobalt, nickel and ruthenium-silica-based materials synthesized by the sol-gel method. *J. Non-Cryst. Solids.* 2008; 354: 4811-4815. <https://doi.org/10.1016/j.jnoncrysol.2008.04.043>
62. Agrafiotis A, Tsetsekou A, Stournaras C.J, Julbe A, Dalmazio L and Guizard C. Evaluation of sol-gel methods for the synthesis of doped-ceria environmental catalysis systems. Part I: preparation of coatings. *J. the Euro. Ceramic Soc.* 2002; 22: 15-25. [https://doi.org/10.1016/S0955-2219\(01\)00246-1](https://doi.org/10.1016/S0955-2219(01)00246-1)
63. Lev O, Tsionsky M, Rabinovich L, Glezer V, Sampath S, Pankaratov I and Gun L. Organically Modified Sol-Gel Sensors. *Anal. Chem.* 1995; 67: 22A-30A. <https://doi.org/10.1021/ac00097a711>
64. Bartholomew C.H and Farrauto R. *J Fundamentals of Industrial Catalytic process*, John Wiley & Sons Inc., Hoboken, New Jersey, (2006).
65. Kortum G. *Reflectance Spectroscopy*, Springer, Berlin, (1969). <https://doi.org/10.1007/978-3-642-88071-1>
66. Skoog D.A, Holler E.J and Crouch. *Instrumental analysis*, India edition, (2008).
67. Brunauer S, Emmett P.H and Teller E. J. Adsorption of Gases in Multi molecular Layers. *Am. Chem. Soc.* 1938; 60: 309-319. <https://doi.org/10.1021/ja01269a023>
68. Rudenberg and Reinhold. Configuration for the enlarged imaging of objects by electron beams. Patent DE905737 (1931).
69. Ernst Ruska. *The Early Development of Electron Lenses and Electron Microscopy*, ISBN-3-7776-0364-3.
70. M. Jag. *Organic spectroscopy principles and applications*. 2nd edition, Norsa publishing House, New Delhi, (2000).
71. M. Thomas and W. J. Thomas. *Principles and Practice of Heterogeneous Catalysis*, 1st edition, New York, (1997).
72. Hayes G.R. and Deveaud B. Is Luminescence from Quantum Wells due to Excitons. *Physica status solidi.* 2002; 190(3): 637-640. [https://doi.org/10.1002/1521-396X\(200204\)190:3<637::AID-PSSA637>3.0.CO;2-7](https://doi.org/10.1002/1521-396X(200204)190:3<637::AID-PSSA637>3.0.CO;2-7)
73. Miditana S.R, Tirukkavalluri S.R, Raju I.M. Synthesis and antibacterial activity of transition metal (Ni/Mn) co-doped TiO₂ nanophotocatalyst on different pathogens under visible light irradiation. *Nanosystems: Phys. Chem. Math.* 2022; 13(1) :104-114. <https://doi.org/10.17586/2220-8054-2022-13-1-104-114>